JOURNAL OF AIRCRAFT
Vol. 39, No. 6, November–December 2002

In-Flight Visualization of Supersonic Flow Transition Using Infrared Imaging

C. P. van Dam* and H. J. Shiu†
University of California, Davis, California 95616
D. W. Banks‡
NASA Dryden Flight Research Center, Edwards, California 93523
and
R. R. Tracy§ and J. Chase¶
Reno Aeronautical Corporation, Carson City, Nevada 89702

Infrared visualization was used to obtain information on the state of the boundary layer of a natural laminar flow airfoil in supersonic flight. In addition to the laminar/turbulent transition boundary, the infrared camera was able to detect shock waves and present a time-dependent view of the flow field. Thermal and flow mechanisms on the surface in flight were modeled numerically to aid in the design of the flight experiment and facilitate analysis of recorded infrared footage. A commercially available infrared camera was adapted for airborne use in this application. Readily available infrared technology has the capability to provide detailed visualization of various flow phenomena in subsonic to hypersonic flight regimes.

Nomenclature

A	=	area
c_f	=	coefficient of skin friction (based on freestream properties)
c_p	=	specific heat at constant pressure
$c_{p,\text{air}}$	=	specific heat at constant pressure of ambient air
$c_{p,\text{skin}}$	=	specific heat at constant pressure of test subject's skin
h	=	flight altitude
k	=	thermal conductivity
M	=	Mach number
Pr	=	Prandtl number
q''	=	rate of heat transfer per unit area
q''_{atm}	=	rate of heat transfer per unit area as a result of diffuse atmospheric heating
q''_{cond}	=	rate of heat transfer per unit area as a result of conduction within test subject
q''_{conv}	=	rate of heat transfer per unit area as a result of convection
q''_{rad}	=	rate of heat transfer per unit area as a result of radiation from test subject
q''_{sol}	=	rate of heat transfer per unit area as a result of solar heating
R	=	recovery factor
T	=	temperature
T_{aw}	=	adiabatic wall temperature
T_w	=	wall (surface) temperature
t	=	time [Pacific Standard Time (PST) unless otherwise noted]
U_∞	=	freestream velocity
V	=	volume
x/c	=	nondimensionalized chord location
α	=	absorptivity
γ	=	ratio of specific heats
ε	=	emissivity
μ	=	absolute viscosity
ρ	=	density
σ	=	Stefan–Boltzmann constant

Subscript

p	=	pressure
∞	=	freestream

Received 11 March 2002; revision received 20 July 2002; accepted for publication 2 August 2002.

*Professor, Department of Mechanical and Aeronautical Engineering, One Shields Avenue; cpvandam@ucdavis.edu. Senior Member AIAA.
†Post-Graduate Researcher, Department of Mechanical and Aeronautical Engineering, One Shields Avenue; hjshiu@ucdavis.edu.
‡Research Scientist, Aerodynamics Branch; dan.banks@dfrc.nasa.gov.
§President, P.O. Box 1404; tracy@renoaero.com. Member AIAA.
¶Engineer, P.O. Box 1404; chaseaero@compuserve.com.

Introduction

EVEN as computer technology evolves and databases of computational fluid dynamics results grow, only flow visualization can offer an accurate and quick portrayal of the actual global flowfield. Flow visualization is a valuable analysis and diagnostic tool that can be employed both in wind tunnels and in flight, verifying performance predictions and revealing flow phenomena in complex, real-world configurations.

Ongoing efforts to improve performance and reduce drag have centered on maintaining laminar flow over airplane surfaces. Recent interests in laminar flow aircraft have included business jets and small and large supersonic and hypersonic applications.[1–5] Verifying the feasibility of such aircraft motivates visualization of boundary-layer transition from laminar to turbulent flow. Boundary-layer visualization also can be beneficially applied toward investigation of high-angle-of-attack flows and devices such as high-lift systems,[6,7] vortex generators, and boundary-layer control systems.

A large variety of instruments and flow-visualization techniques exists for study of boundary-layer transition on aircraft surfaces including oil flow,[8] sublimating chemicals,[9,10] liquid crystals,[11,12] surface oil film interferometry,[13] temperature-sensitive paints,[14] hot-film anemometry,[2,6,7,12,15,16] thermocouples,[12] microphones,[15] total pressure (Preston) tubes,[17] and infrared sensors.[2,6,7,12,18–20] Many of these methods are intrusive, introducing measurement hardware or substances on to the subject surface that can inhibit natural flow development. Hot films, thermocouples, microphones, and Preston tubes, while providing excellent quantitative data, involve the most complex installations and provide strictly localized information. Liquid crystals, temperature-sensitive paints, and pressure-sensitive

paints, while providing global information, require extensive surface preparation and employ substances that might require specialized protocols for both application and removal. Oils and sublimating chemicals are generally confined to one condition per application, limiting their utility in flight experimentation. Infrared, however, is nonintrusive and continuously provides global surface flow information over a range of conditions. Depending on the subject, minimal or no surface treatment might be necessary.

Most applications of infrared in flow visualization have been limited to wind-tunnel applications where conditions can be strictly controlled. Boundary-layer transition and separation have been visualized in wind-tunnel tests using actively heated airfoil models constructed of an insulative material.[21] Temperature changes as low as 0.02 K at transition have also been detected on models without active heating.[22]

In-flight experiments have been successful with local installation of an infrared imaging system; that is, the infrared camera is installed within the aircraft being studied.[2,6,7,18–20] Obviously, visualization is limited solely to the aircraft in which the camera is installed. Local installations might require extensive modification to the subject aircraft, including relatively expensive infrared-transparent windows of germanium, zinc sulfide, or zinc selenide. The field of view is also restricted, limiting the areas of the aircraft that can be studied and, especially with smaller aircraft, resulting in images captured at extremely oblique angles.

Many of these shortcomings can be addressed by locating the infrared camera remotely. With remote imaging the camera is no longer installed on the subject aircraft being studied. The camera can be ground-based, as in recent experiments with Ballistic Missile Defense Organization infrared telescopes and the space shuttle.[23] Alternatively, the camera can also be in flight on another aircraft, as in the Infra-Red Imagery of Shuttle (IRIS) experiments performed during hypersonic reentry with the Kuiper Airborne Observatory and the space shuttle,[24] and the Forward Looking Infra-Red (FLIR) pod on NASA Dryden Flight Research Center's (DFRC) F/A-18 #846 used to image the flow over a T-34C and a Learjet Model 24.[25–27]

Locating the camera remotely eliminates the need for extensive modifications to each subject aircraft under study. Additionally, by strategically selecting the subject's flight path and attitude relative to the camera, limitations in field of view associated with locally mounted cameras are mostly eliminated. Different parts of a subject aircraft can be studied during the same flight, and more favorable viewing angles can be obtained. However, the freedom in position between the subject and camera introduces new complications in imaging.

This paper presents the results of a recent flight investigation of a supersonic natural laminar flow wing using infrared imaging. Initially the plan was to use the DFRC F/A-18 #846 with the FLIR pod to remotely visualize the test article via infrared. However, a portion of the test envelope was outside the flight envelope of the F/A-18, and, hence, a local installation was selected. To minimize expense, infrared camera selection was limited to preexisting installations or commercially available systems adapted for airborne use. The data were stored on videotape and then digitized for further analysis. In the following section the methodology and approach used in the flight investigation are discussed. Next, a numerical model is introduced to aid in the design and analysis of infrared flight experiments. The supersonic flight results are then detailed, and future plans for quantitative data analysis are outlined.

Methodology and Approach

As with any imaging visualization application, the study of the supersonic natural laminar flow airfoil can be divided into two primary components: the imaging system and the test subject. In this investigation the imaging system and subject were mounted on the same airplane, an F-15B.

Infrared Imaging System

To explore the feasibility of utilizing an IR imaging system to support visualization studies, an initial series of tests were conducted using an AN/AAS-38 NITE Hawk targeting pod mounted on a chase aircraft. The targeting pod, installed on the port side of DFRC F/A-18 #846, provided a stabilized infrared imaging capability in the 8–12 micron spectral band. Initial data acquired with the system indicated that IR thermography was a very promising tool for flow visualization.[25–27] The presence of fixed pattern noise and other residual effects of the scanned image required extensive postprocessing to minimize the impact on the accuracy of the experimental data.

For the next phase of the investigation, a modified version of the NITE Hawk targeting pod equipped with a 3–5 micron focal plane array sensor was utilized. Experimental results obtained with this sensor indicated improved sensitivity and resolution. The primary limitation of this method was the ability to position the experiment and chase aircraft sufficiently close to each other and with the sightline angle required to acquire the region of interest.[27]

For the investigation discussed in this paper, the proven 3–5 micron staring sensor was deployed in an externally mounted pod, located on the experimental airplane with a fixed line of sight, centered on the region of interest. The imaging system is based on a Raytheon Radiance HS camera. The camera utilizes an Indium-Antimonide (InSb) focal plane with a 256 × 256 array of 30-micron pixels. The sensor responds in the 3–5 micron spectral range. A 13-mm lens was selected to capture a complete view of the experiment with minimal background within the field of view. The imaging system was packaged within a pod mounted on the starboard side armament rail of a F-15B, as shown in Fig. 1. For this first phase of the investigation, the images were stored as analog video on Hi-8 videotape. Storage of the data on video results in an increase in signal noise and tends to preclude conversion of the data into surface temperatures. A system upgrade to store the images digitally is currently underway and will allow more intensive image processing and quantitative data analysis.

To minimize the size of the pod and resultant drag, the sensor was oriented parallel to the airflow. This also placed the line of sight parallel to the experiment. A fold mirror was incorporated in the design to fold the line of sight inboard and down to center on the region of interest (Fig. 2). A silicon window with an antireflection coating optimized for the 3–5 micron spectral band was installed on the inner surface of the pod directly in front of the fold mirror.

To further minimize the volume of the pod, the camera electronics were installed in an adjacent airplane bay with an interface cable connection to the camera head. The electronics package provides simultaneous National Television System Committee (NTSC), Luminance/Chrominance (Y/C), and 12-bit digital output. The camera operational settings can be adjusted on the ground prior to flight through an RS-422 computer interface. The system was equipped

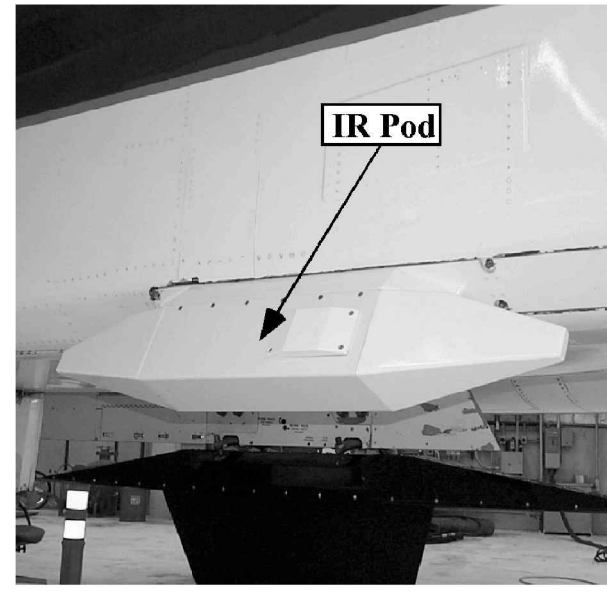

Fig. 1 Infrared pod mounted on starboard armament rail of NASA F-15B airplane.

with test ports and cables to enable external configuration and test support without the need for aircraft power.

Test Article

The test article was designed to mount to the centerline store station of the F-15B, as shown in Fig. 3. The test article has a tapered planform and biconvex section shape and is fabricated out of aluminum 6061-T6. Insulating material was applied over much of the surface to reduce the effects of heat conduction into the test article. The leading and trailing edges were not insulated because of the lack of thickness available in those areas. The insulating material consisted primarily of aluminum impregnated epoxy and syntactic foam. Details on determining the type and amount of insulation applied are discussed in the following section. However, the geometric details of the test article must remain proprietary at this point in time.

F-15B Test Bed

The F-15B is a two-seat version of the F-15A, a high-performance, supersonic, all-weather air-superiority fighter built by McDonnell-Douglas Aircraft Company (now the Boeing Company). The supersonic natural laminar flow test article was mounted on the centerline tank location of NASA DFRC F-15B #836. The fixture did not limit the airplane's flight envelope, nor was there significant performance degradation as a result of the test article. The airplane is outfitted with a flight-test nose boom in order to obtain accurate air data during flight.[28]

Numerical Prediction of Surface Temperature

The temperature distribution on the test article was predicted using numerical methods to provide a basis for surface insulation selection and the required temperature range and sensitivity of the infrared imager used in this application as well as to evaluate the effect of transient flight conditions.

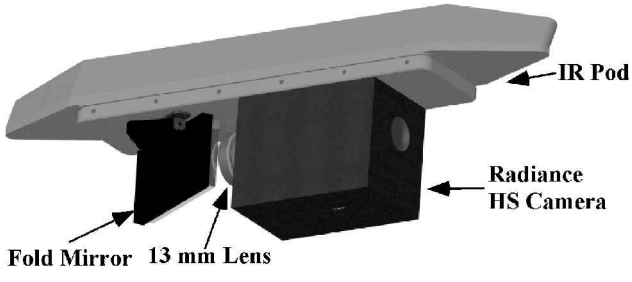

Fig. 2 Infrared camera system inside pod.

Methodology

Assuming a wing section with little taper and sweep, the spanwise temperature gradient is small, and a two-dimensional model is adequate. The wing is discretized into chordwise and depthwise segments. The temperature distribution is determined through heat-transfer calculations. Heat transfer is governed by the first and second laws of thermodynamics. For this application the first law can be expressed as

$$\frac{\partial}{\partial t}\iiint_V \rho c_p T \, \mathrm{d}V = -\iint_A q'' \, \mathrm{d}A \tag{1}$$

As illustrated in Fig. 4, there are five significant sources of heat transfer at each wing segment:

$$\frac{\partial}{\partial t}\iiint_V \rho c_{p,\mathrm{skin}} T \, \mathrm{d}V = -\iint_A (q''_{\mathrm{conv}} + q''_{\mathrm{rad}} + q''_{\mathrm{sol}} + q''_{\mathrm{atm}} + q''_{\mathrm{cond}}) \, \mathrm{d}A \tag{2}$$

q''_{conv} is the convective heat transfer as a result of flow over the wing. The convective heat transfer is dependent on skin friction, as follows[29]:

$$q''_{\mathrm{conv}} = (c_f/2)\rho_\infty U_\infty (T_W - T_{\mathrm{aw}})(k/\mu)Pr^{\frac{1}{3}} \tag{3}$$

At low Mach numbers the adiabatic wall temperature is effectively equal to the freestream total temperature. However, as Mach number increases the recovery factor R can make a notable contribution to the adiabatic wall temperature:

$$T_{\mathrm{aw}} = T_\infty + R\left(U_\infty^2 \big/ 2c_{p,\mathrm{air}}\right) = T_\infty\left\{1 + R[(\gamma - 1)/2]M_\infty^2\right\} \tag{4}$$

Because the recovery factor differs in laminar and turbulent boundary layers, the recovery factor influences the surface temperature gradient between laminar and turbulent walls at higher Mach numbers.

q''_{rad} is the heat transfer as a result of radiation from the wing surface:

$$q''_{\mathrm{rad}} = \varepsilon\sigma T_w^4 \tag{5}$$

ε is emissivity, a surface property that relates the maximum possible heat flux to the actual heat flux emitted by a body. It is dependent on factors such as material, surface finish, and surface color. Given emissivity, surface temperature distributions can be deduced

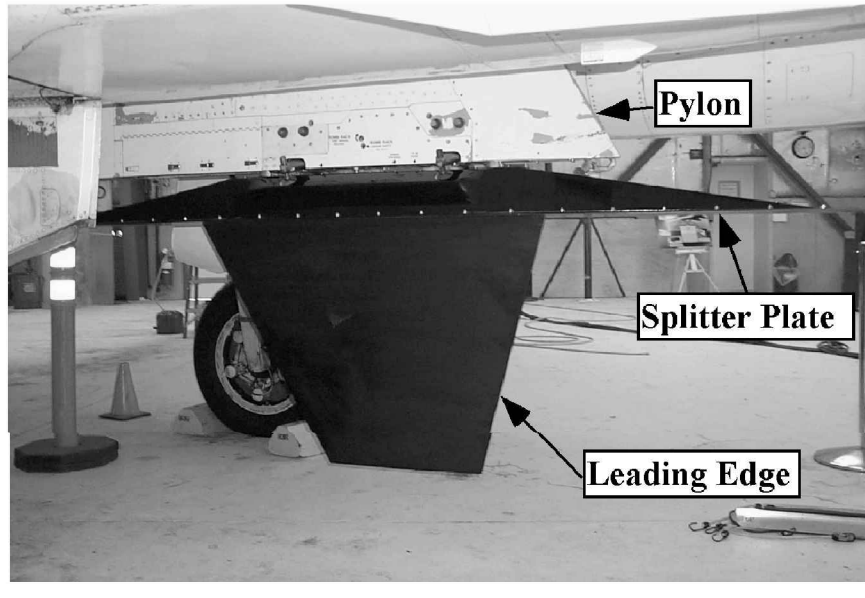

Fig. 3 Supersonic laminar flow test article mounted on NASA F-15B airplane.

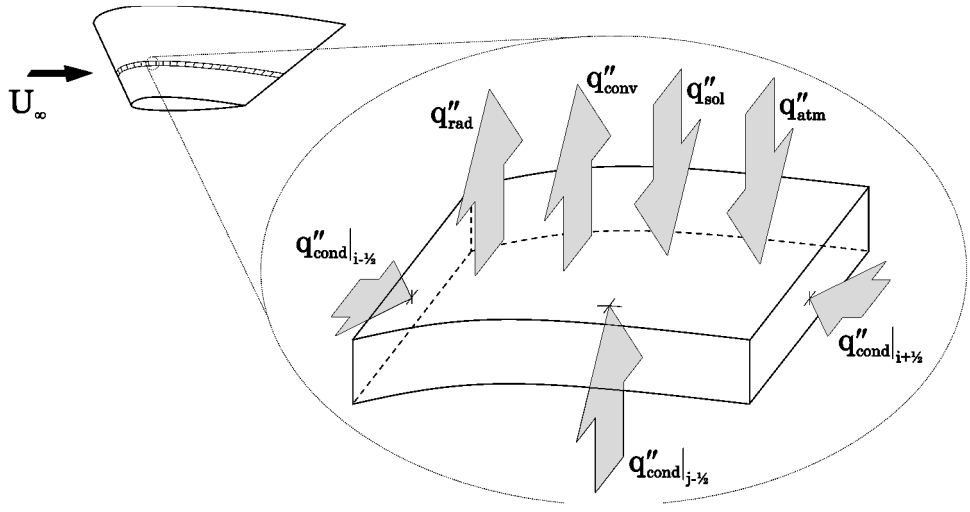

Fig. 4 Heat-transfer mechanisms on a wing element in flight.

from radiation measurements such as those performed with infrared detectors.

Currently, q''_{sol} is estimated as a constant value of 1300 W/m^2 when the surface is exposed to the sun. Direct solar heating is assumed to be negligible and is set to zero when the surface is shaded from the sun, as with the test article in this experiment.

As a radiation term, q''_{atm} is expressed similarly as the wing surface radiation component in Eq. (5):

$$q''_{atm} = \alpha\sigma T_\infty^4 \tag{6}$$

In this equation α is absorptivity, a surface property analogous to emissivity. Absorptivity relates the maximum possible heat flux into a body to the actual heat absorbed by the body.

q''_{cond} is the heat conduction within the wing skin and internal structure. Fourier's law states that

$$q''_{cond} = -k\nabla T \tag{7}$$

The formulation in Eq. (2) was implemented to solve both steady-state and time-dependent cases. The steady-state model is solved iteratively. The time-dependent model is solved using the backward Euler method with a time step determined through a solution accuracy requirement. The test article is geometrically symmetric and is assumed to also be thermally symmetric. It is therefore modeled as a half-section with adiabatic conditions at the centerline. The half-section is discretized into 100 chordwise segments and six depthwise segments.

Subsonic and transonic skin-friction values were numerically determined with MSES, a viscous-inviscid interaction method for the aerodynamic analysis of airfoils.[30] Supersonic skin-friction values were based on the local temperature and calculated via linear theory and an empirical two-dimensional flat plate formulation with a compressibility correction.[31] Laminar and turbulent recovery factors were set as follows: $R_{laminar} = 0.85$, $R_{turbulent} = 0.88$.[32] Atmospheric properties were assumed to be standard.

Of the five heat-transfer sources just listed, convective heat transfer, solar heating, and surface conduction are the dominant mechanisms in the present experiment. Analysis of the temperatures for a range of flight conditions indicates that the most significant source of heat input can come from direct solar heating creating hot-wall conditions relative to the adiabatic wall temperature. Hot-wall conditions in combination with the skin-friction difference between laminar and turbulent flows results in laminar surfaces having higher temperatures than turbulent surfaces. Interesting enough, the difference between the laminar and turbulent recovery factors has an opposite effect with laminar surfaces encountering slightly less heating as a result of compressibility than turbulent surfaces. One reason to develop the preceding temperature prediction method was to evaluate the effect of these counteracting phenomena on surface temperature gradients. A second reason was to obtain a better understanding of the normal and tangential heat-conduction effects on the temperature gradients at transition and the types of surface insulation to apply. Lastly, insight into transient effects of Mach number and altitude changes on surface temperature provided by the method aided in the development of suitable flight-test profiles.

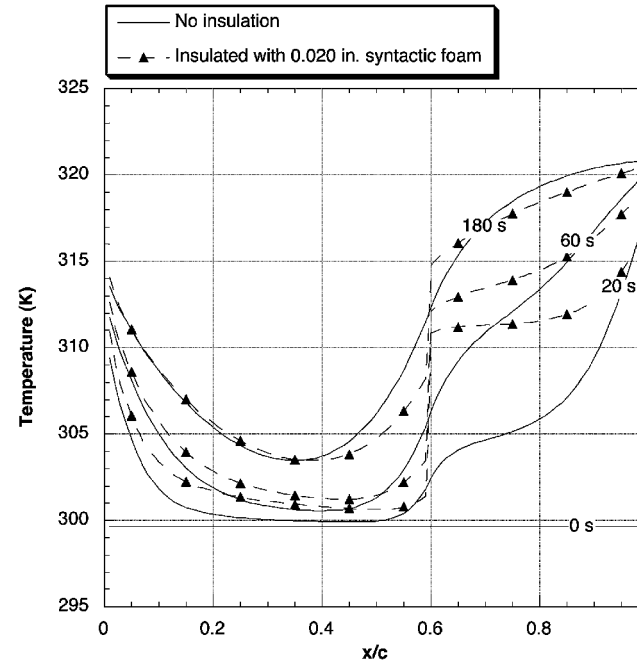

Fig. 5 Temperature distribution history with 0.020-in. syntactic foam. Three percent biconvex airfoil; M_∞ = 1.4; h = 24,500 ft (standard atmosphere); uniform initial temperature of 300 K. Transition at 60% of chord.

Temperature Predictions

Several cases were investigated with thin-skinned and solid-bodied wings at subsonic, transonic, and supersonic conditions through various flight profiles.[27] Sample results and some important conclusions are presented next. All results indicated the importance of considering heat conduction within the wing structure. Even in cases where the wing surface was modeled as a thin skin with an adiabatic inner surface, chordwise conduction sometimes smears temperature distributions, shifting and weakening the surface temperature gradient between the laminar and turbulent boundary layers.

Figure 5 shows surface temperature distributions on a wing with boundary-layer transition specified at 60% of chord. In this case the

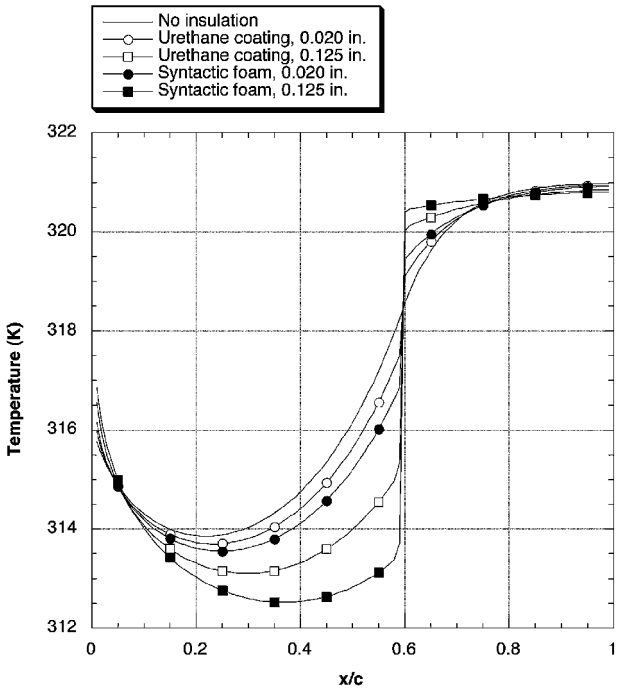

Fig. 6 Steady-state surface temperature distributions with insulation. Three percent biconvex airfoil M_∞ = 1.4; h = 24,500 ft (standard atmosphere); uniform initial temperature of 300 K. Transition at 60% of chord.

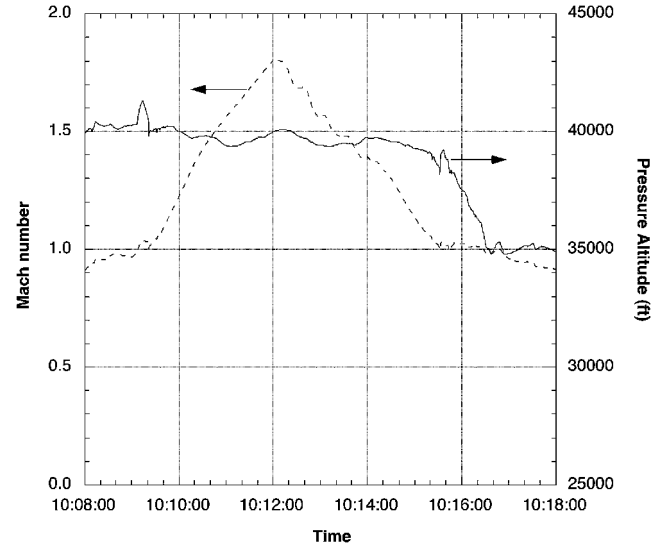

Fig. 7 Flight 152 profile in terms of the pressure altitude and freestream Mach number.

wing is modeled as solid aluminum, in accordance with the actual test article. Transition location is difficult to discern by inspection of the temperature distribution of the noninsulated wing.

The addition of a thin layer of insulation on the surface can inhibit conduction of heat into the wing structure, thereby improving the temperature gradient at the transition location and, consequently, aiding transition detection. Figure 5 also shows the beneficial effect of the addition of a layer of insulation and reveals the time-dependent nature of temperatures at the wing surface. Again, the insulation mitigates the surface conduction effect, improving transition detection by establishing a strong temperature gradient at the transition location.

In preparing the test article for investigation of supersonic natural laminar flow, several thicknesses and types of insulation were investigated. Steady-state results are shown in Fig. 6. These results and corresponding time-dependent solutions show that increased thicknesses of insulation better preserve surface temperature gradients. However, insulation thickness is practically limited by structural constraints. Given the thin test article used in these experiments, a 0.060 in. layer of syntactic foam was selected as insulation.

Flight Results and Discussion

This section presents and discusses flow-visualization results obtained from flight tests of the natural laminar flow wing test article at supersonic speeds. A natural laminar flow wing is designed to maintain extended runs of laminar flow without active means such as suction. The visualizations presented and discussed here were digitized using an Apple Power Macintosh G4 and Media 100 digital video editing hardware and software. Contrast stretching was applied where indicated. Contrast stretching involves redistribution of the intensity levels within an image to emphasize key regions of interest. Intensity gradients can therefore be amplified. Some caution must be applied with contrast stretching. Because the redistribution of intensities does not have to be linear, important features can be suppressed, and insignificant features can be falsely inflated. Other than contrast stretching, no image processing was performed on the images.

The data summarized in this section were acquired during five flight tests. During these flights, each data run lasted approximately 10 min, during which the airplane was accelerated to supersonic speed, held at predetermined conditions, and then decelerated to subsonic speed. The test course was chosen to optimize the sun angle (minimize or eliminate direct solar radiation on the test article and avoid reflections back to the camera) for the IR imaging while remaining within the supersonic test corridor. Flights were conducted up to Mach 2.0 and up to pressure altitudes of 45,000 ft. A typical flight-test profile in terms of the freestream Mach number and pressure altitude as a function of time is depicted in Fig. 7. Four of the flights were conducted with the test article having a leading-edge sweep angle of 15 deg and a trailing-edge sweep angle of 30 deg as depicted in Fig. 3. To evaluate the effect of increased leading-edge sweep on the flow development over the test article, one flight was conducted with the article rotated 180 deg about its spanwise axis. For several of the tests, cylindrical flow trips were attached to the test article in the tip region. The trips were approximately 0.25 in. (6.35 mm) in diameter and 0.010 in. (0.25 mm) high.

The infrared images in Fig. 8 are taken from Flight 152 with trips installed on the test article. Time is expressed in hours:minutes:seconds. This is the actual time of the day of the flight test in PST for Flights 151 and 152 and PDT for Flight 168. Lighter intensities mark warmer regions, and darker intensities mark cooler regions. Figure 8c shows the test article with significant features indicated. The four tooling marks indicated are jigging holes in the aluminum substrate beneath the surface insulation layer that were required during manufacturing of the test article. As expected, the noninsulated leading and trailing edges are distinctly visible.

Before 10:10:00, as the F-15 climbed to a nominal pressure altitude of 40,000 ft and accelerated to supersonic speeds, the entire test article surface was of approximately uniform intensity. The surface pattern shown in Fig. 8a at 10:10:02 ($M_\infty = 1.24$) faded in over a period of about 5 s. The lighter intensity wedges off the trips suggest that the warmer, lighter surfaces are turbulent and that laminar flow extends over the entire chord across the full span except for the most inboard region. As the airplane continues to accelerate, the transition front is seen advancing toward the leading edge, the wedges disappear, and the entire insulated surface becomes a relatively light intensity, signifying a completely turbulent surface at 10:10:10 and $M_\infty = 1.30$, as shown in Fig. 8b.

A gradual progression of laminar flow with increasing Mach number begins almost immediately afterwards, as shown in Fig. 8b ($M_\infty = 1.33$ at 10:10:14) to Fig. 8f ($M_\infty = 1.76$ at 10:11:49). The insulated surface is warmer than the noninsulated leading and trailing edges, which is consistent with the numerical calculations. The turbulent wedges off the two installed trips are visible starting in Fig. 8c. As in Fig. 8a and as numerically predicted, the turbulent boundary-layer region is warmer.

After reaching the maximum Mach number at approximately 10:12:00, the airplane decelerated at constant altitude, and the transition location gradually and smoothly returned forward. At 10:13:09 and $M_\infty = 1.55$ in Fig. 8g as well as at 10:14:19 and $M_\infty = 1.34$ in Fig. 8h, the transition is still distinct, but the difference in intensities of the laminar and turbulent regions is no longer as obvious. This is a transient effect caused by the decreasing Mach number. As the Mach number decreases, the difference in the turbulent and laminar wall temperature decreases. The freestream total temperature also decreases, and the test article, retaining heat from the previous flight condition, becomes warmer relative to the adiabatic wall temperature. If the adiabatic wall temperature is lower than the surface temperature of the test article, the temperature gradient at transition reverses. Solar radiation, which is not entirely blocked by the F-15′s fuselage, can also heat the test surface article, helping accelerate the reversal. By 10:14:28 in Fig. 8i, the effect of the deceleration is complete, and the turbulent surface is cooler than the laminar surface. The surface is fully turbulent by 10:14:41.

Almost immediately after, starting at 10:14:43 ($M_\infty = 1.23$), the surface pattern shown in Fig. 8j appears. The test article is showing

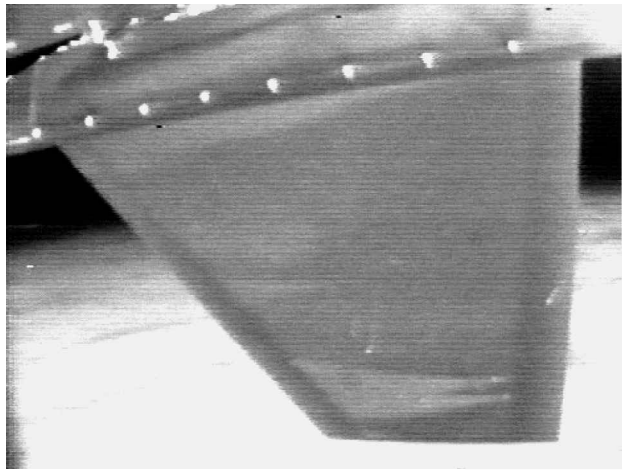

a) $t = 10{:}10{:}02$, $h_p = 39{,}989$ ft, $M_\infty = 1.24$ (contrast stretching applied)

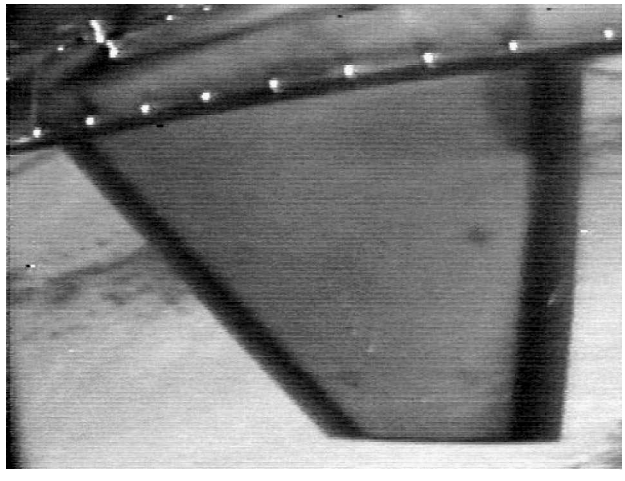

b) $t = 10{:}10{:}14$, $h_p = 39{,}764$ ft, $M_\infty = 1.33$ (contrast stretching applied)

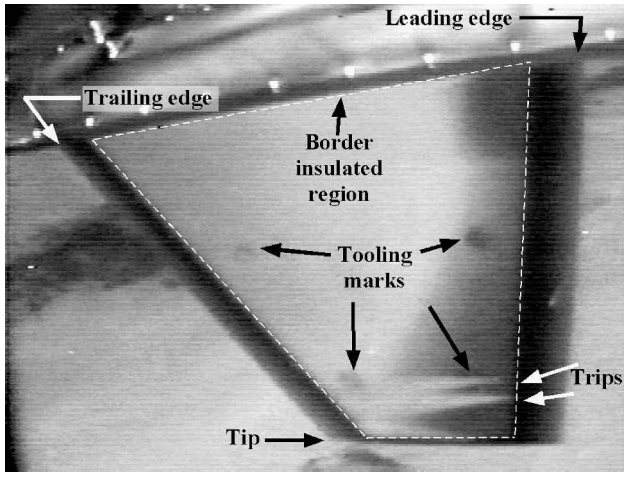

c) $t = 10{:}10{:}27$, $h_p = 39{,}793$ ft, $M_\infty = 1.41$ (contrast stretching applied)

d) $t = 10{:}10{:}38$, $h_p = 39{,}788$ ft, $M_\infty = 1.47$

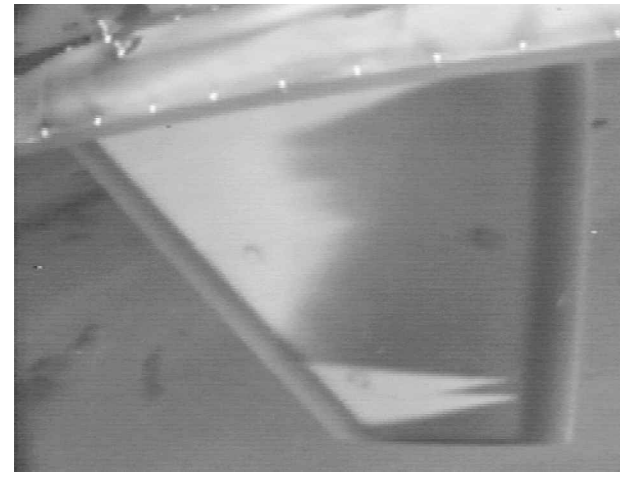

e) $t = 10{:}10{:}57$, $h_p = 39{,}450$ ft, $M_\infty = 1.55$

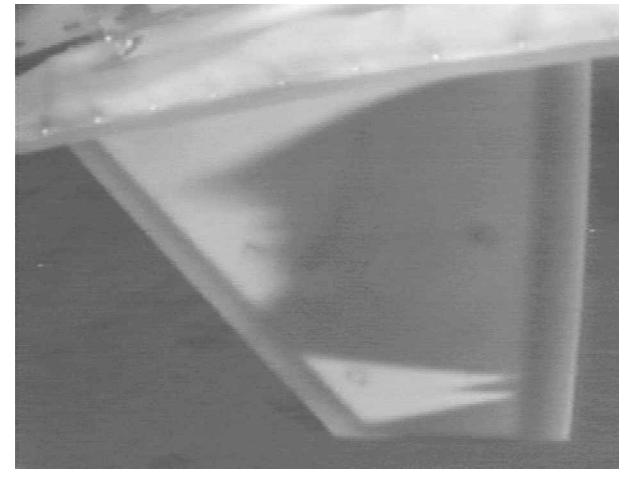

f) $t = 10{:}11{:}49$, $h_p = 39{,}764$ ft, $M_\infty = 1.76$

Fig. 8 Infrared image of test article during Flight 152.

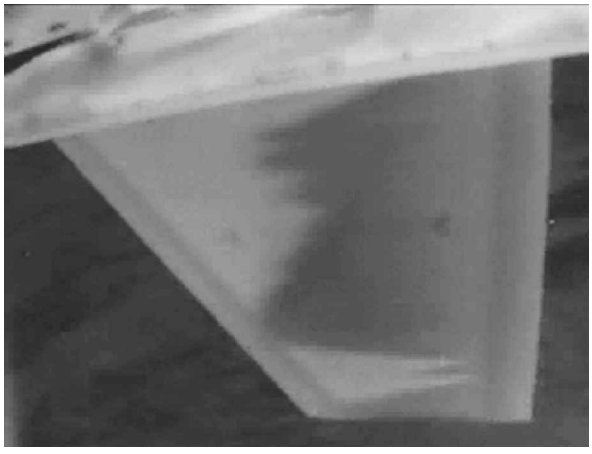

g) $t = 10{:}13{:}09$, $h_p = 39{,}372$ ft, $M_\infty = 1.55$

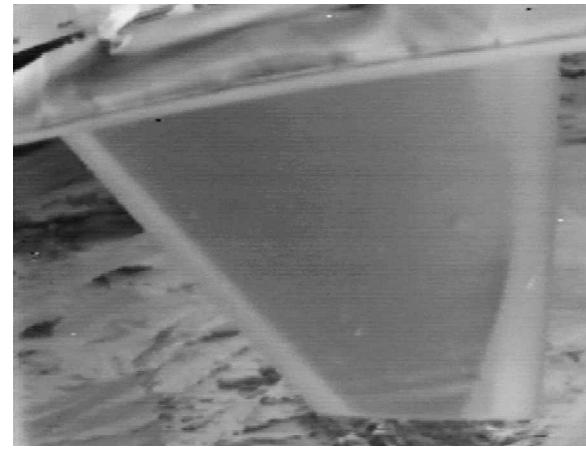

i) $t = 10{:}14{:}28$, $h_p = 39{,}586$ ft, $M_\infty = 1.31$

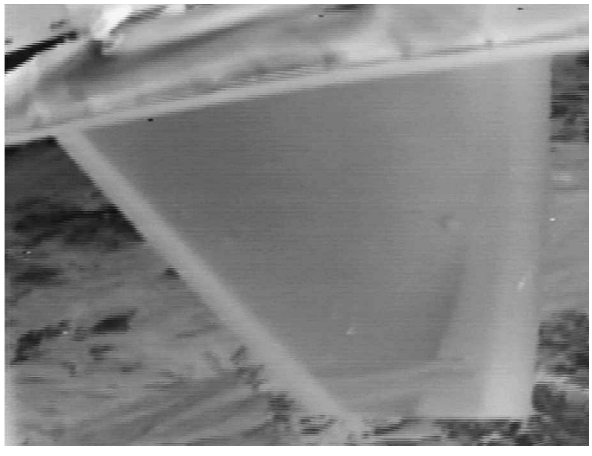

h) $t = 10{:}14{:}19$, $h_p = 39{,}680$ ft, $M_\infty = 1.34$

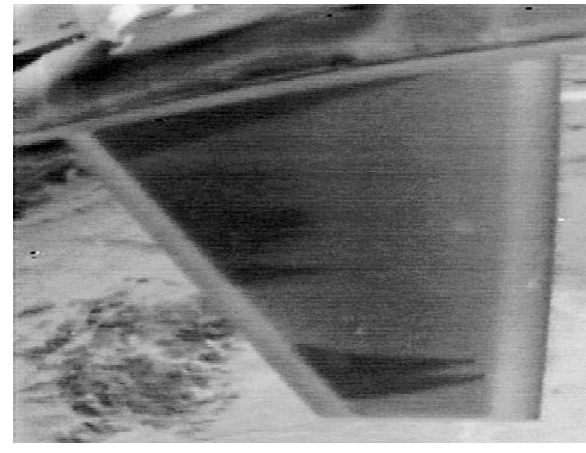

j) $t = 10{:}14{:}49$, $h_p = 39{,}506$ ft, $M_\infty = 1.23$ (contrast stretching applied)

Fig. 8 Infrared image of test article during Flight 152 (continued).

significant laminar flow again. The surface pattern is nearly identical to that shown in Fig. 8a, except reversed, and occurs at approximately the same flow conditions.

The disturbance of flow on a surface from an unforeseen shock off a more forward body is a well-documented issue with supersonic aircraft.[33] Initially it was theorized that a shock system originating from the IR pod (Fig. 1) was the source of the surface pressure disturbance leading to the observed movement of transition with Mach number. However, recent analyses using an inviscid (Euler) flow solver indicate that a shock system originating in the leading-edge region of the pylon and wrapping around the splitter plate appears to be the main source of pressure disturbance. Figure 3 shows the splitter plate separating the airplane pylon and test article. The test article's thin geometry and sharp leading edge create favorable pressure gradients at supersonic conditions, encouraging laminar flow. At $M_\infty = 1.24$ in Fig. 8a, nearly the entire surface is laminar. The surface becomes fully turbulent at $M_\infty = 1.30$, as the shock from the pylon crosses on to the test article surface, inducing transition. As the Mach number increases, the shock pressure disturbance and transition location both move aft.

In Fig. 8f at $M_\infty = 1.76$, laminar flow has extended well beyond the shock location. By applying extreme contrast stretching, shown in Fig. 9, a darker intensity arc is visible within the laminar flow region. In Fig. 10, taken from an earlier flight at almost identical conditions, different camera settings allow the arc to be seen more clearly. The combination of the increasingly stable boundary layer at higher Mach numbers and the gradual diffusion of the shock as it extends further from the pylon allows the boundary layer to extend downstream of the intersection of the shock cone.

In Figs. 8g–8j the F-15 decelerates, and the shock intersection and transition location return forward. In Fig. 8j the shock sweeps off the leading edge of the test article, and the surface becomes fully laminar again.

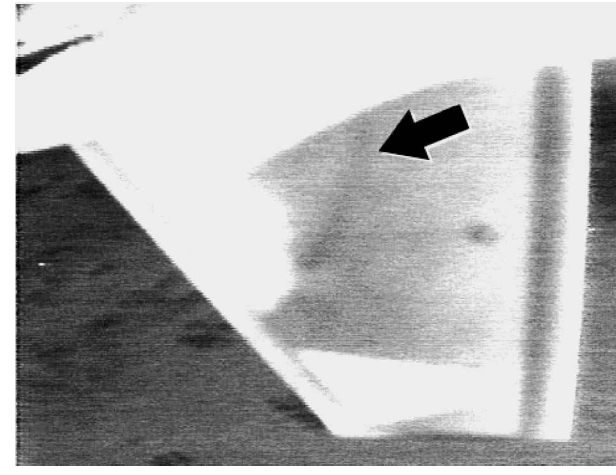

Fig. 9 Infrared image of test article during Flight 152: $t = 10{:}11{:}49$, $h_p = 39{,}764$ ft, $M_\infty = 1.76$. This image is identical to Fig. 8f but with contrast stretching applied. The arrow marks a shock.

Finally the test article was reversed to provide a 30-deg-leading-edge sweep during the fourth flight. Figure 11 shows an image taken during this flight. As in the other flights, a transition front can be seen at approximately midchord. Furthermore, a turbulent wedge can be seen propagating from the leading edge near the test article tip. The source of this transition was a surface imperfection on the leading edge of the article.

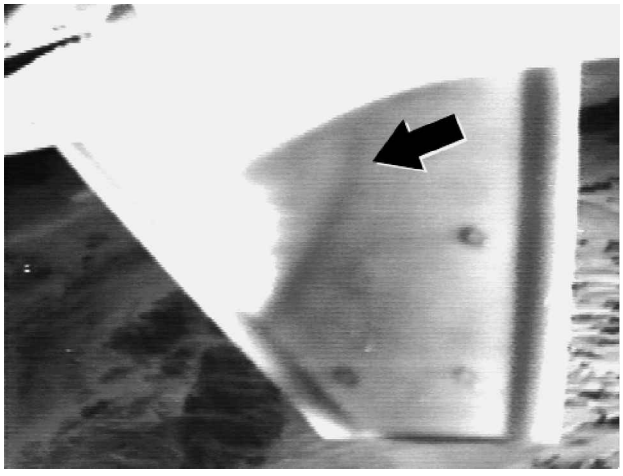

Fig. 10 Infrared image of test article during Flight 151: t = 10:15:59, h_p = 39,600 ft, M_∞ = 1.71. Contrast stretching applied. The arrow marks a shock.

Fig. 11 Infrared image of test article during Flight 168: t = 10:02:11(PDT), h_p = 39,500 ft, M_∞ = 1.59.

Conclusions

The use of infrared imaging to visualize a supersonic flow field and define transition boundaries has been demonstrated. In addition to identifying boundary-layer transition, the infrared images have been able to identify shock waves impinging on the surface of the test article. Video sequences are able to reveal time-dependent processes. The images presented were acquired and stored on Hi-8 tape and later digitized. Once implemented, these systems can rapidly acquire data throughout a wide range of flight conditions.

The temperature prediction procedure allows us to evaluate the effects of transient flight conditions, solar heating, heat conduction, and other phenomena on the surface temperature distribution. The results of these simulations provide insight into the need as well as the type and amount of surface insulation needed for in-flight infrared imaging. The structural and surface design of the test article is an important consideration in obtaining meaningful data from infrared systems.

The data presented here were collected on Hi-8 videotape using the Y/C output from the camera. These data were then digitized after collection for further analysis. An upgrade to acquire and store the images digitally is currently in progress. In subsequent tests the camera's full 12-bit signal will be captured and stored. These digital images will likely provide additional detail of these types of flowfields. The recording system will support continuous collection of the digital data for up to two hours. Data collection can be started and stopped using a cockpit control switch. Flight data are downloaded postflight to a portable FireWire hard drive at approximately three times the real-time recording rate. The portable drive can be connected to a computer workstation or network for long-term storage or analysis. The acquisition of raw digital data will allow more intensive image processing and more detailed, quantitative temperature analysis. Other aerodynamic phenomena can potentially be visualized using infrared thermography, such as flow separation or vortical flows. It is only necessary to create a temperature difference larger than about 0.025 K that can be differentiated by the sensor.

Acknowledgments

The efforts at the University of California, Davis, were supported by the NASA Dryden Flight Research Center under cooperative agreements NCC4-114, NCC4-120, and NCC4-151. We thank Patrick Morrison for his help with the data reduction.

The tests described herein were planned and conducted cooperatively under a memorandum of understanding between NASA Dryden Flight Research Center and Reno Aeronautical Corporation. The test article was privately designed and developed by Reno Aeronautical Corporation and Directed Technologies, Inc., in Arlington, VA. Ilan Kroo and Peter Sturdza of Stanford University, California, performed the transition analyses essential to the test article design. Prior supersonic laminar flow application studies and subsequent flight tests were supported in part by Defense Advanced Research Projects Agency.

References

[1]Tracy, R., "High Efficiency, Supersonic Aircraft," U.S. Patent 5,322,242, June 1994.

[2]Voogt, N., "Flight Testing of a Fokker 100 Test Aircraft with Laminar Flow Glove," *Transitional Boundary Layers in Aeronautics*, edited by R. A. W. M. Henkes and J. L. van Ingen, North-Holland, Amsterdum, 1996, pp. 39–51.

[3]Bertelrud, A., and Graves, S., "Transition in Flight at Supersonic and Hypersonic Mach Numbers," *Transitional Boundary Layers in Aeronautics*, edited by R. A. W. M. Henkes and J. L. van Ingen, North-Holland, Amsterdum, 1996, pp. 423–432.

[4]Kroo, I., Sturdza, P., Tracy, R., and Chase, J., "Natural Laminar Flow for Quiet and Efficient Supersonic Aircraft," AIAA Paper 2002-0146, Jan. 2002.

[5]Wlezien, R., and Veitch, L., "Quiet Supersonic Platform Program," AIAA Paper 2002-0143, Jan. 2002.

[6]Yip, L. P., van Dam, C. P., Whitehead, J. H., Hardin, J. D., Miley, S. J., Potter, R. C., Bertelrud, A., Edge, D. D., and Willard, P. E., "The NASA B737-100 High-Lift Program—Measurements and Computations," *The Aeronautical Journal*, Vol. 99, No. 989, 1995, pp. 372–386.

[7]Van Dam, C. P., Los, S. M., Miley, S., Roback, V. E., Yip, L. P., Bertelrud, A., and Vijgen, P. M. H. W., "In-Flight Boundary-Layer Measurements on a High-Lift System: Slat," *Journal of Aircraft*, Vol. 34, No. 6, 1997, pp. 748–756.

[8]Curry, R. E., Meyer, R. E., and O'Connor, M., "The Use of Oil for In-Flight Flow Visualization," NASA TM 84915, Jan. 1984.

[9]McTigue, J. G., Overton, J. D., and Petty, G., Jr., "Two Techniques for Detecting Boundary-Layer Transition in Flight at Supersonic Speeds and at Altitudes above 20,000 Feet," NASA TN D-18, Aug. 1959.

[10]Obara, C. J., "Sublimating Chemical Technique for Boundary-Layer Flow Visualization in Flight Testing," *Journal of Aircraft*, Vol. 25, No. 6, 1988, pp. 493–498.

[11]Holmes, B. J., Gall, P. D., Croom, C. C., Manuel, G. S., and Kelliher, W. C., "A New Method for Laminar Boundary Layer Transition Visualization in Flight—Color Changes in Liquid Crystal Coatings," NASA TM 87666, Jan. 1986.

[12]Hall, R. M., Obara, C. J., Carraway, D. L., Johnson, C. B., Wright, R. E., Jr., Covell, P. F., and Azzazy, M., "Comparisons of Boundary-Layer Transition Measurement Techniques at Supersonic Mach Numbers," *AIAA Journal*, Vol. 29, No. 6, 1991, pp. 865–879.

[13]Drake, A., and Kennelly, R. A., "In-Flight Skin Friction Measurements Using Oil Film Interferometry," *Journal of Aircraft*, Vol. 36, No. 4, 1999, pp. 723–725.

[14]Cattafesta, L. N., III, and Moore, J. G., "Transition Detection in High-Speed Flows with Luminescent Temperature-Sensitive Paint," *Flow Visualization VII*, edited by J. Crowder, Begell House, New York, 1995, pp. 944–949.

[15]Greff, E., "In-Flight Measurement of Static Pressures and Boundary-Layer State with Integrated Sensors," *Journal of Aircraft*, Vol. 28, No. 5, 1991, pp. 289–299.

[16]Van Dam, C. P., Los, S. M., Miley, S., Roback, V. E., Yip, L. P., Bertelrud, A., and Vijgen, P. M. H. W., "In-Flight Boundary-Layer Measurements on a High-Lift System: Main Element and Flap," *Journal of Aircraft*, Vol. 34, No. 6, 1997, pp. 757–763.

[17]Yip, L. P., Vijgen, P. M. H. W., Hardin, J. D., and van Dam, C. P., "In-Flight Pressure Measurements on a Subsonic Transport High-Lift Wing Section," *Journal of Aircraft*, Vol. 32, No. 3, 1995, pp. 529–538.

[18]Brandon, J. M., Manuel, G. S., Wright, R. E., and Holmes, B. J., "In-Flight Flow Visualization Using Infrared Imaging," *Journal of Aircraft*, Vol. 27, No. 7, 1990, pp. 612–618.

[19]Quast, A., "Detection of Transition by Infrared Image Technique," *Proceedings of the International Congress on Instrumentation in Aerospace Simulation Facilities Record*, Inst. of Electrical and Electronics Engineers, New York, 1987, pp. 125–134.

[20]Horstmann, K. H., Redeker, G., Quast, A., Dreßler, U., and Bieler, H., "Flight Tests with a Natural Laminar Flow Glove on a Transport Aircraft," AIAA Paper 90-3044, Aug. 1990.

[21]Gartenberg, E., and Roberts, A. S., Jr., "Airfoil Transition and Separation Studies Using an Infrared Imaging System," *Journal of Aircraft*, Vol. 28, No. 4, 1991, pp. 225–230.

[22]Bouchardy, A., Durand, G., and Gauffre, G., "Processing of Infrared Thermal Images for Aerodynamic Research," *Proceedings of the International Society for Optical Engineering*, Geneva, Switzerland, Vol. 397, April 1983, pp. 304–309.

[23]Blanchard, R. C., Wilmoth, R. G., Glass, C. E., Merski, N. R., Berry, S. A., Bozung, T. J., Tietjen, A., Wendt, J., and Dawson, D., "Infrared Sensing Aeroheating Flight Experiment: STS-96 Flight Results," AIAA Paper 2001-0352, Jan. 2001; also *Journal of Spacecraft and Rockets*, Vol. 38, No. 4, 2001, pp. 465–472.

[24]Green, M. J., Budnik, M. P., Yang, L., and Chiasson, M. P., "Supporting Flight-Data Analysis for Space-Shuttle Orbiter Experiments at NASA Ames Research Center," NASA TM 84345, April 1983.

[25]Van Dam, C. P., Shiu, H. J., and Banks, D. W., "In-Flight Flow Visualization Using Infrared Thermography," NASA CR-97-207087, Nov. 1997.

[26]Van Dam, C. P., Shiu, H. J., and Banks, D. W., "Remote In-Flight Boundary Layer Transition Visualization Using Infrared Thermography," *Proceedings of the 8th International Symposium on Flow Visualization*, edited by G. M. Carlomagno and I. Grant, Paper 181, 1998 (CD ROM, ISBN 0953399109).

[27]Shiu, H. J., "Remote In-Flight Boundary Layer Visualization via Infrared Imaging," Master's Thesis, Dept. of Mechanical and Aeronautical Engineering, Univ. of California, Davis, 2000.

[28]Richwine, D. M., "A Test Bed for Flight Research Experiments," AIAA Paper 97-2293, June 1997.

[29]Incropera, F. P., and DeWitt, D. P., *Introduction to Heat Transfer*, 2nd ed., Wiley, 1990, p. 345.

[30]Drela, M., "Newton Solution of Coupled Viscous/Inviscid Multielement Airfoil Flows," AIAA Paper 90-1470, June 1990.

[31]Eckert, E. R. G., "Engineering Relations for Heat Transfer and Friction in High-Velocity Laminar and Turbulent Boundary-Layer Flow over Surfaces with Constant Pressure and Temperature," *Transactions of the ASME*, Vol. 78, No. 6, 1956, pp. 1273–1283.

[32]Shapiro, A. H., *The Dynamics and Thermodynamics of Compressible Fluid Flows*, Ronald, New York, 1953, p. 1126.

[33]Anders, S. G., and Fischer, M. C., "F-16XL-2 Supersonic Laminar Flow Control Flight Test Experiment," NASA TP-1999-209683, Dec. 1999.